Exploring the Impact of Morphology on the Properties of Biodegradable Nanoparticles and Their Diffusion in Complex Biological Medium

Ridolfo, Roxane

2021-01

Ridolfo , R , Tavakoli , S , Junnuthula , V , Williams , D S , Urtti , A & van Hest , J C M 2021 , ' Exploring the Impact of Morphology on the Properties of Biodegradable Nanoparticles and Their Diffusion in Complex Biological Medium ' , Biomacromolecules , vol. 22 , no. 1 , pp. 126-133 . https://doi.org/10.1021/acs.biomac.0c00726

http://hdl.handle.net/10138/325594
https://doi.org/10.1021/acs.biomac.0c00726

BioMACROMOLECULES

pubs.acs.org/Biomac

Article

Exploring the Impact of Morphology on the Properties of Biodegradable Nanoparticles and Their Diffusion in Complex Biological Medium

Roxane Ridolfo, Shirin Tavakoli, Vijayabhaskarreddy Junnuthula, David S. Williams,* Arto Urtti,* and Jan C. M. van Hest*

Cite This: *Biomacromolecules* 2021, 22, 126−133

Read Online

ACCESS | Metrics & More | Article Recommendations | Supporting Information

ABSTRACT: Nanoparticle morphology (size, shape, and composition) and surface chemistry are the determining factors underpinning the efficacy of such materials in therapeutic applications. The size, shape, and surface chemistry of a nanoparticle can strongly influence key properties such as interactions with diverse biological fluids and interfaces and, in turn, impact the delivery of bioactive cargo, modulating therapeutic performance. This is exemplified in ocular drug delivery, where potential therapeutics must navigate complex biological media such as the gel-like vitreal fluid and the retina. Biodegradable block copolymer amphiphiles are a robust tool for the engineering of various types of self-assembled nanoparticles with diverse morphologies ranging from spherical and tubular polymersomes to spherical and worm-like micelles. Here, we explore the effect of morphological features such as shape and surface chemistry upon the interactions of a series of copolymer nanoparticles with retinal (ARPE-19) cells and the release of a low solubility drug (dexamethasone) that is currently used in ocular therapy and study their diffusion *in vitreous* using *ex vivo* eyes. We demonstrate that both aspect ratio and surface chemistry of nanoparticles will influence their performance in terms of cell uptake, drug release, and diffusion with high aspect ratio shapes demonstrating enhanced properties in relation to their spherical counterparts.

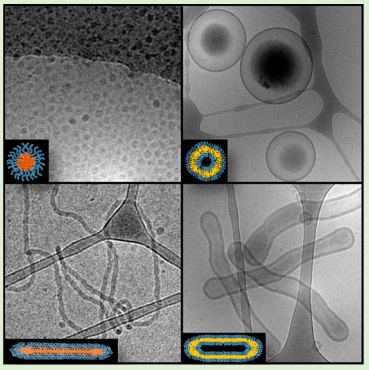

INTRODUCTION

The important role of nanoparticle morphology for performance of such synthetic materials in a biological context is a well-established concept.[1] Greater understanding of the influence that certain morphological features (such as size, shape, and composition) can have upon complex biological interactions, and associated properties such as drug release, will aid in developing design principles to engineer next-generation nanotechnologies that might overcome current limitations in the field.[1−3] However, due to the inherent heterogeneity of biology (not only at the level of organs and tissues but also with respect to cell types and subcellular systems), there cannot be a "one-size-fits-all" approach to nanomedicine.[4,5] The impact of nanoparticle morphology may well be quite different depending upon the niche application and biological context, which necessitates customized *in vitro* and *in vivo* assays to provide specific insights toward the target.[6−8]

Ocular therapy (in contrast to areas such as neurological or immunological therapy) possesses a host of unique biological challenges peculiar to the biology of the eye.[9] Drug administration to the eye is complicated, especially when the posterior segment has to be targeted. Neither topical (eye drops) nor systemic treatments effectively reach the back of the eye due to significant ocular barriers such as the blood−retinal barrier or the natural elimination processes. This is usually overcome using intravitreal injections, an unpleasant procedure that could be lessened by the development of controlled release technology, increasing the interval between treatments.[10−12] In terms of disease specifics, a condition like age-related macular degeneration (AMD) is a worldwide disease that is on the rise in an aging population.[13] AMD is now a top ten priority for the World Health Organization (WHO), and patient numbers are expected to reach 288 million by 2040, motivating the development of new treatments.[14,15] AMD is caused by age-related degeneration of retinal pigmented epithelium (RPE) cells in the central region of the retina (the macula) that can lead to accumulation of extracellular material and inflammation.[16] Intravitreal injection is the only appropriate treatment modality that exists, which requires a good understanding of how drug delivery is affected by the vitreous in which the administration takes place. The vitreous fluid within the eye is a complex

Special Issue: Bioinspired Macromolecular Materials

Received: May 11, 2020
Revised: June 4, 2020
Published: June 8, 2020

medium, accounting for 80% of the eye volume, which comprises collagen fibers and hyaluronic acid, making it a gel-like, viscous liquid.[17] In addition, the inner limiting membrane (ILM) of the retina forms a physical barrier for drug delivery to retinal cells.

Nanoparticle morphology has been shown to significantly influence properties such as circulation times, cell interactions, and flow behavior.[18−22] In terms of ocular therapy, particle surface charge has been shown to influence permeation in the vitreous, with positive charge-bearing particles showing enhanced diffusion without crossing the inner retinal membrane.[10,23−25] In contrast, neutral and negatively charged macromolecules and nanoparticles showed some permeation across the inner limiting membrane, demonstrating a possibly enhanced delivery to cells.[10,24,25] The potential of nanoparticles to impact drug delivery, particularly in ocular therapy, is highly appealing, and morphology has a key role in realizing this.

The anti-inflammatory corticosteroid, dexamethasone (DEX), is a frontline therapeutic for ocular therapy. As with many drug molecules, DEX has poor water solubility owing to its hydrophobic nature, which limits administration to the retina at doses necessary for effective therapy (ca. 150 μg/mL over 2 months).[26] Without formulation, DEX must be given as an aggregated suspension that provides rapid drug release and necessitates daily intravitreal injection. Current strategies to improve DEX delivery include intravitreal implants (e.g. Ozurdex, Allergan) that can provide sustained release for 6 months.[27] However, this implant previously showed unwanted complications such as movement from the back to the front segment of the eye, affecting vision, which therefore requires surgical removal.[28] This opens an opportunity for nanomedicine to provide a competitive solution.[10] In general, the design of nanoparticles, particularly those comprising biodegradable copolymers, for application in ocular therapy is an unexplored area.

Here, we explore the key properties of a range of nanoparticle morphologies comprising biocompatible, amphiphilic block copolymers in relation to cell viability and uptake, drug (DEX) release, and diffusion *in vitreous*. Based on previously reported systems, we utilized spherical and worm-like micelles, comprising poly(ethylene glycol) (PEG) and combinations of poly(trimethylene carbonate) (PTMC) and poly(ε-caprolactone) (PCL), as well as spherical and tubular polymersomes, comprising PEG and poly(D,L-lactide) (PDLLA).[29−32] Using a range of physical characterization techniques and biological assays, we demonstrated that particle shape and composition have a significant effect upon performance to direct cellular interactions, control drug release, and enhance diffusion in vitreous (using an *ex vivo* eye model). Overall, our findings highlight the value of high aspect nanoparticles such as tubes and worms and the potential for nonspherical particles to improve the performance of nanotherapeutics. To the best of our knowledge, this is the first report that systematically compares the biological impact of such diverse morphologies arising from copolymer self-assembly. In these terms, our findings will not only be of use for ocular delivery but for broader therapeutic applications of such nanomaterials.

MATERIALS AND METHODS

Materials. All chemicals were used as received unless otherwise stated. PEG initiators were purchased from Rapp Polymere GmbH (Germany) and JenKem Technology (United States). Fluorescent BDP-FL-COOH was supplied by Lumiprobe. All other chemicals were supplied by Sigma-Aldrich (Merck). Porcine eyes were supplied by Lassa slaughterhouse (Finland). Vitreal fluid was collected from porcine eyes as reported in the literature.[33] Ultrapure Milli-Q water was obtained from a Labconco Water Pro PS purification system (18.2 MΩ) and used for all aqueous solutions. ARPE-19 cells and related medium were obtained from ATCC/LGC Standards. Details of all instrumentation used for particle characterization can be found in the Supporting Information.

Polymer Synthesis and Nanoparticle Formulation. Polymer synthesis and particle fabrication were conducted as previously described.[30,31] Reaction schemes and polymer characterization data can be found in Figures S1−4. Fluorescent polymers were prepared by conjugation with Bodipy-FL-CO_2H dye via esterification (Figure S5). The resulting nanoparticles were characterized using a combination of AF4, DLS, and CryoTEM. Addition of charge-bearing block copolymers was performed by mixing either amino (A)-modified or carboxylic acid (CA)-modified copolymer with unmodified (U)-copolymer at 10 wt % ratio (Figures S1 and S2). For confocal imaging, fluorescent particles with equivalent sizes were obtained by mixing BODIPY-copolymer with unmodified polymer at 10 or 50 wt %, respectively, for micellar or vesicular systems (equivalent to 0.1 or 0.5 mg/mL of dye-labeled polymer for a total polymer mass of 1 mg/mL).

Drug Encapsulation. The hydrophobic corticosteroid dexamethasone (DEX) was used in this study. DEX loading of particles was presented in terms of total mass in relation to the mass of the copolymer. For polymersomes, encapsulation efficiency was determined using UPLC. Two hundred microliters of particles was evaporated in a 1 mL Eppendorf tube using a vacuum centrifuge for 2 h at 60 °C. The dried powder was subsequently dissolved in a 1:40 mix of THF:ACN, and any undissolved matter was removed by centrifugation at 6 krcf for 10 min (DEX dissolves in this solvent mixture). The supernatant solution (containing DEX) was diluted 50% with Milli-Q water and analyzed with UPLC using a ACQUITY HSS T3 column (100 Å, 1.8 μm, 2.1 × 50 mm, C18) at a flow rate of 0.01 mL/min with elution peaks appearing at 0.73 min for all measurements (conducted in triplicate). Drug encapsulation efficiencies (EE) were calculated as follows:

$$\mathrm{EE\%} = \frac{[\mathrm{DEX}]_{\mathrm{UPLC}}}{[\mathrm{DEX}]_0} \times 100$$

For micellar morphologies, encapsulation efficiency was determined using UV−visible spectroscopy. Ten microliters of a polymer stock was hydrated (as nanoparticles) into PBS, and 10 μL of the same stock was dissolved in ACN. The sample dissolved in organic solvent was considered the reference, containing 100% of DEX (no self-assembly occurred in the reference solvent). Nanoparticle solutions in PBS were filtered (0.2 μm PES filter), and 500 μL was transferred to a 5 mL Eppendorf tube and freeze-dried overnight. After drying, 1 mL of a 1:1 mixture of ACN:water was added, and the resulting solution was centrifuged to remove undissolved salts. The supernatant was then diluted 4 times before measuring the absorbance of DEX at 240 nm. DEX concentration was calculated from a DEX calibration curve in the same solvent ($y = 14.41x$ with $R^2 = 0.999$). Samples hydrated by PBS ($[\mathrm{DEX}]_{\mathrm{PBS}}$) were compared with samples in organic solvent ($[\mathrm{DEX}]_{\mathrm{ACN}}$) as a reference (Figure S11). Drug loading efficiencies were calculated as follows:

$$\mathrm{EE\%} = \frac{[\mathrm{DEX}]_{\mathrm{PBS}}}{[\mathrm{DEX}]_{\mathrm{ACN}}} \times 100$$

Drug Release. Drug release studies were performed using a Rapid Equilibrium Dialysis (RED) device with 8K MWCO inserts as supplied by Thermo Fisher Scientific. The donor chamber contained 250 μL of sample and 250 μL of buffer (with 25 μL premixed Pen-Strep antibiotic). The receiving chamber contained 750 μL of PBS. Aliquots of 100 μL were extracted from the receiving chamber at specific time points, and 100 μL of PBS was pipetted in replacement

https://dx.doi.org/10.1021/acs.biomac.0c00726
Biomacromolecules 2021, 22, 126−133

to maintain sink conditions. To each aliquot, 400 μL of acetonitrile was added to dilute the sample and precipitate any salts prior to centrifugation at 6 krcf for 10 min. Fifty microliters of supernatant was then withdrawn and dissolved in Milli-Q water at a 1:1 volume ratio. Each of three replicates was measured by UPLC (dilution factor 10) to determine the [DEX]. The cumulative release of DEX (%) was calculated as follows, with $[DEX]_t$ the measured concentration at time t and 12.5 the dilution factor (total volume of 1250 μL/sample volume 100 μL), where M_t is mass of drug in the device, and Q_t is cumulative mass of drug released:

$$M_t = ([DEX]_t \times 0.1\ \text{mL}) \times 12.5$$

$$Q_t = Q_{t-1} + \left[M_t - M_{t-1}\left(1 - \frac{1}{12.5}\right)\right]$$

Cell Assays. ARPE-19 cells were cultured at 37 °C in 5% CO_2 using DMEM:F12 medium. Cells were plated at 2×10^5 cells per well and treated with nanoparticle formulations at 3 different polymer concentrations (1.25, 0.625, and 0.250 mg/mL) for 24 h. After incubation with particles, cells were washed several times with DPBS. To measure health, cells were treated with 10% Alamar Blue solution and incubated for 4 h, and the absorbance at 570 nm was recorded thereafter. To measure proliferation, cells were incubated for 3 days without particles. Thereafter, 10 μL per well of CCK-8 solution was added, and microplates were incubated for an additional 3 h before absorbance was read at 450 nm.

Cellular Uptake Assays. ARPE-19 cells were plated on either 24-well plates or special glass coverslips at 2×10^5 cells per well and treated with 1 mL of fluorescently labeled nanoparticles in DMEM:F12 at 1 mg/mL for 24 h. After incubation, cells were washed several times with DPBS and processed using either flow cytometry or confocal microscopy.

For flow cytometry, 1 mL of medium was added per well together with 5 μg/mL of Hoechst 33342 nuclear stain. After 30 min of incubation, cells were washed 3 times with DPBS, trypsinized, and resuspended in DPBS. The resulting cell suspensions were transferred to FACS tubes for analysis. For confocal microscopy, cells were fixed by incubation using 1 mL per well of 4% paraformaldehyde solution in DPBS for 15 min. Once washed, staining was achieved using 300 μL of 0.2% Triton in DPBS per well for 10 min, followed by 3 DPBS rinses and addition of 300 μL of Phalloidin 568 per well. After 45 min, 5 washing steps using 500 μL of TWEEN solution per well (0.2% in DPBS) were performed, waiting 5 min between repeats. Finally, cells were rinsed with DPBS, treated with 300 μL of DAPI solution per well for 5 min, and rinsed before imaging.

Mobility Studies *in Vitreous* Using *ex Vivo* Eyes. Mobility studies of nanoparticles *in vitreous* were performed using porcine eyes *ex vivo*.[34] To prepare the eyes, they were cleaned from muscles, nerves, and all other undesired tissues. Freshly prepared eyes were briefly dipped into 70% ethanol and then stored in PBS at 4 °C overnight. Thereafter, eyes were cut circumferentially below the limbus to remove the anterior section, including iris and lens. A 30G syringe was used to inject (in the fresh eye vitreous) 50 μL of fluorescent nanoparticles at a polymer concentration of 0.25 mg/mL. Next, the cut surface was covered with a microwell dish (MatTek Corporation, Ashland, MA, United States), avoiding air bubbles between the vitreous and the glass window. The eye cup was then inverted to place the window surface facing down for imaging.

The key parameter for mobility evaluation was the ratio of particle diffusion coefficient (as described in the Stokes−Einstein equation) in water (D_W) compared to that *in vitreous* (D_V): D_w/D_V (Figure S13). D_W was calculated at 37 °C in water, using DLS. To compensate for the inaccuracies relating to the hydrodynamic radius of tubular polymersomes, approximations based on the diffusion of rod-like particles were used rather than standard calculations based upon spherical shapes.[35] Mobility of particles in vitreous fluid was recorded as a movie with 50 ms temporal resolution, and particles were tracked using single particle tracking technique. From the videos, the mean square displacement (MSD) value was computed using the @MSDanalyzer MATLAB plugin in Imaris 9.2 software based on the equation $MSD(\Delta t) = 4D_V\Delta t$ for 2D particle tracking (Figure S13B).[33]

Retinal Explant Preparation and Immunohistochemistry. Fresh bovine eyes were obtained from a local slaughterhouse (Eastern Finland), and the retinal explants were prepared according to a published method.[36] Surrounding connective tissues were removed, and the eye was dipped shortly in 20% ethanol. To expose the neural retina in the posterior segment, first, the eyeball was bisected and the anterior segment was discarded followed by vitreous removal. Next, the eye cup was filled with CO_2 independent medium (Gibco, Thermo Fisher Scientific, United States) and cut by scissors to make four flaps. Circular section of the retina was isolated using a tissue puncture blade, and two explants were placed on a 75 mm Transwell insert where the explant was nourished by culture medium (Neurobasal-A, 2% B-27 supplement, 2% penicillin−streptomycin, 1% L-glutamine; all Gibco, Thermo Fisher Scientific, United States). Ten microliters of Bodipy-FL-labeled CA-tubes (3 mg/mL) was placed gently on top of the explant and incubated for 24 h at 37 °C with 5% CO_2. The next day, the medium was replaced with 4% paraformaldehyde (PFA) to fix the retinal explant. After 2 h of incubation at 4 °C, PFA was removed and replaced by 30% sucrose in PBS and incubated overnight at 4 °C. Retinal explants were snap frozen in O.C.T (Tissue-Tek Sakura) using liquid nitrogen. Cryosections (16 μm) were obtained by cutting from four different area of the explant with cryostat (Leica CM3050s). Retinal sections were incubated in 50 μL of blocking solution (5% goat serum) for 1 h at RT followed by overnight incubation with rabbit antibody against Collagen IV (1:200) (ab6586, Abcam, United States) at 4 °C to tag the ILM. The next day, sections were stained with secondary antibody (Alexa Fluor 568-labeled goat antirabbit secondary antibody, A11036, Thermo Fisher Scientific, OR, United States) and Hoechst at 10 μg/mL concentration (33342, Invitrogen, Thermo Fisher, United States) for 1 h at RT. Lastly, retinal sections were covered with mounting medium (Vectashield, Vector Laboratories, CA, United States) and kept at 4 °C until imaging. Sections were imaged with a confocal microscope (Leica TCS SP8) using 20× (HC PL APO) and 93× (HC PL APO) objectives.

RESULTS AND DISCUSSION

To engineer various nanoparticle morphologies, we synthesized a range of well-defined block copolymers comprising PEG, PTMC, PCL, and PDLLA in various combinations, using procedures presented in our previous reports (Figures S1−S5).[29−32] To enable further study into the impact of surface chemistry upon performance, copolymers with PEG-terminal amine (A) and carboxylic acid (CA) moieties were also prepared and blended with unmodified (U) polymers for assembly into A- and CA-bearing particles. Spherical and tubular polymersomes were fabricated using our protocols where 10 wt % of A or CA groups could be stably incorporated, yielding particles with sizes around 450 (U/A) or 250 nm (CA) (Figures S6). Zeta potentials of U/CA-spheres or -tubes were ≈−45 mV and those of A-spheres/tubes were ≈−25 mV owing to the presence of surface amine moieties amidst PEG polymers. Spherical and worm-like micelles were fabricated using our protocols where 10 wt % of A or CA groups could be stably incorporated with sizes ≈30 nm for spherical and ≈150 nm for worm-like micelles. Zeta-potentials of spherical U/CA-micelles were approximately −5 mV, whereas for A-micelles they were ≈4 mV; values for U/CA-worms amounted to −17 mV and A-worms ≈7 mV (Figure S7). Particle sizing was conducted using DLS, with the elongated particle (tube or worm) diameter calculated as if it was spherical (based on Stokes−Einstein equation), and cryo-TEM imaging provided detailed structural features of these

https://dx.doi.org/10.1021/acs.biomac.0c00726
Biomacromolecules 2021, 22, 126−133

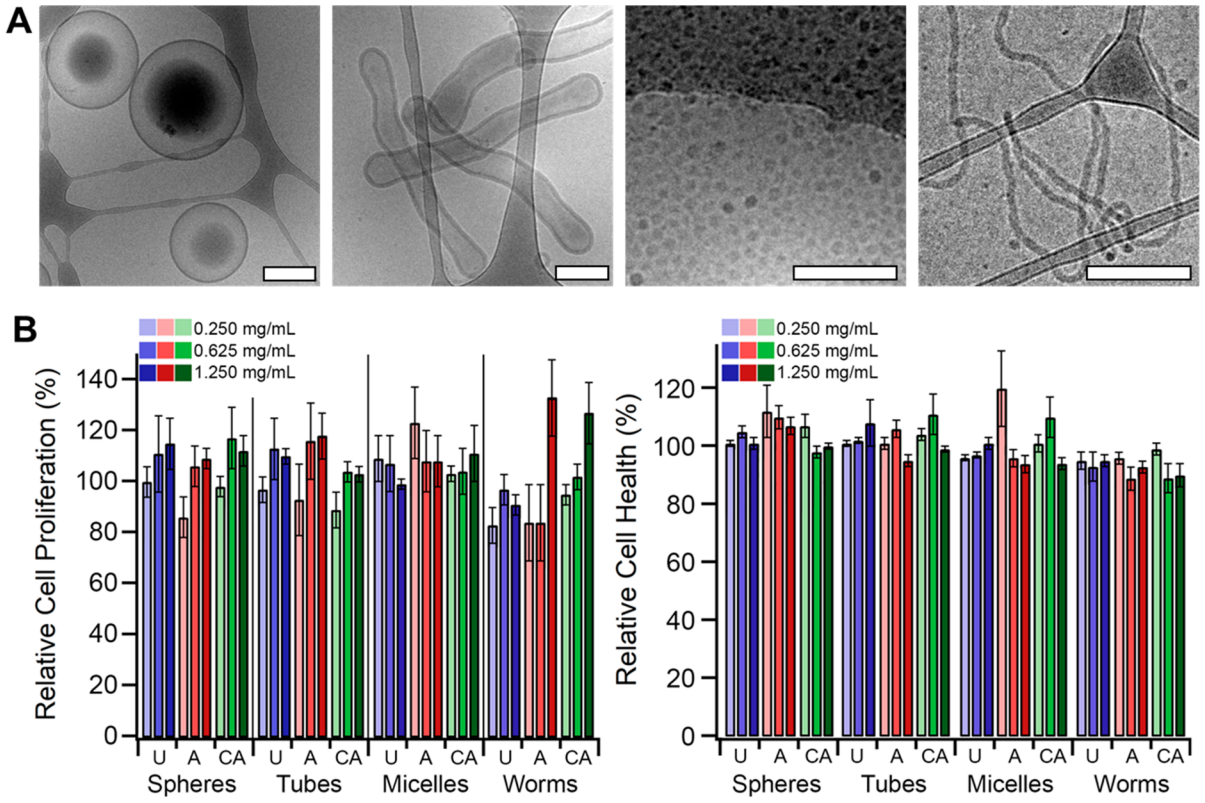

Figure 1. Biocompatible block copolymer nanoparticles and their effect on retinal (ARPE-19) cells. (A) Cryo-TEM images of unmodified polymersomes, tubes, micelles, and worms (left to right, scale bars = 0.2 μm). Images of nanoparticles with different surface compositions available in Figure S8. (B) Relative proliferation (CCK-8) and health (Alamar Blue) values of retinal cells after 24 h incubation with increasing concentrations of diverse nanoparticles with unmodified (U), 10% amine-modified (A), or 10% carboxylic acid-modified (CA) surfaces.

diverse nanoparticles (Figures 1A and S8). High aspect ratio structures (tubes and worms) possess lengths >1 μm and widths of around 100 or 50 nm, respectively.

Using a retinal pigmented epithelial cell line (ARPE-19), no significantly detrimental effect was observed upon cell viability or proliferation using Alamar blue and CCK-8 assays, respectively, arising from treatment with any of the nanoparticle candidates (Figure 1B). Interestingly, some reduction in viability was observed in cell proliferation after treatment with tubes and worms at lower concentrations (to a minimum of 80%), but this did not bear out at higher concentrations and was not of sufficient magnitude to be of concern. Using confocal microscopy and flow cytometry, cellular uptake was confirmed in each case (Figure 2A and B, S9, and S10).[37] Overall, tubes were more readily taken up by cells as compared to their spherical counterparts by ca. 20% (Figure 2A). In terms of surface composition, it was clear from flow cytometry results that A-spheres/tubes were less readily taken up. This result was somewhat counterintuitive as the introduction of positive charge on the nanoparticle surface should induce a favorable interaction with the negatively charged plasma membrane.[38] In our system, this difference was related to the tendency of amine-modified spheres/tubes to bind to and aggregate on the cell membrane, hindering efficient internalization (evidenced in Figure S9C/Videos 1−6). Uptake of U- and CA-tubes was optimal in terms of the relative number of cells that contained nanoparticles (as presented in flow cytometry data). In contrast, there was a strong difference between the uptake of spherical and worm-like micelles with almost twice the number of cells containing worms (Figure 2B). In this case, there was no significant impact arising from surface composition, and all three worm systems showed increase cell uptake. This distinct uptake behavior was likely caused by the enhanced diffusive properties of high aspect ratio structures, which was more intense in the case of worms due to their greater length:width aspect ratio as compared to that of tubes.

Another important property of such nanoparticles is their ability to release encapsulated drug, and the effect that their unique morphologies have on this property has not yet been explored. There were key distinctions, in terms of drug loading, between nanoparticles under examination. PEG−PDLLA polymersomes, formed via solvent switch and (in the case of tubes) with dialysis-induced shape transformation possessed a low loading of DEX at around 0.5 wt % (yielding a total concentration of ca. 25 μg/mL, see Supporting Information). In contrast, micellar technology was capable of higher drug loadings at up to 4 wt % (spherical micelles) or 10 wt % (worm-like micelles) owing to the molecular structure of PEG−PTMC/PCL copolymers and the direct hydration process, yielding total concentrations of 180 and 500 μg/mL, respectively (Figure S11). Release of DEX from polymersomes, diluted using vitreous liquid, proceeded under first order kinetics. In contrast to free drug, which rapidly equilibrated across the system within 6 h (k_1 = 0.55 h^{-1}, Figure S12A), release from polymersomes was slowed, albeit with a distinct impact arising from shape upon the rate constant (Figures 2C and S12B). In each case there was a 20−30% reduction in the rate constant of drug release in the tubular as compared to spherical polymersomes. In terms of release from the micellar

https://dx.doi.org/10.1021/acs.biomac.0c00726
Biomacromolecules 2021, 22, 126−133

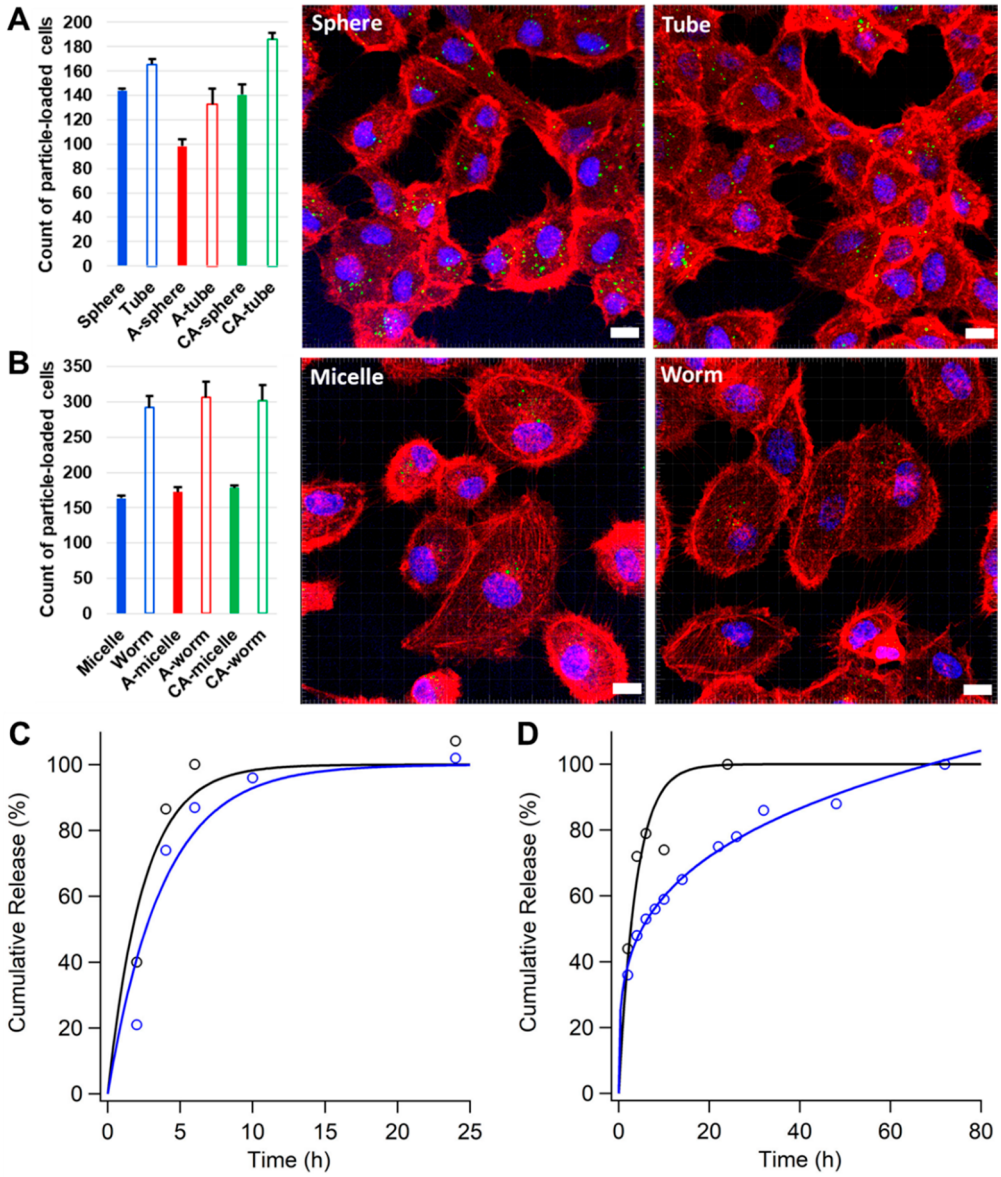

Figure 2. Effect of nanoparticle morphology upon uptake in retinal (ARPE-19) cells and the release of a low solubility drug (dexamethasone). Uptake of (A) spherical and tubular polymersomes and (B) spherical and worm-like micelles into cells as quantified using flow cytometry accompanied by confocal microscopy (cytoplasm = red, nucleus = blue, nanoparticles = green, and scale bars = 10 μm). (C) Cumulative release of DEX from spherical (black) and tubular polymersomes (blue) fitted using first-order kinetics (full analysis on all polymersome samples available in Figure S12). (D) Cumulative release of DEX from spherical (black) and worm-like micelles (blue) fitted using first-order and Korsmeyer−Peppas kinetics, respectively (full analysis on all micelle samples is available in Figure S12).

particles, although spherical micelles exhibited first order release, comparable to that from tubular polymersomes, a striking difference was observed when studying worm-like morphologies (Figures 2D and S12C). DEX release from worms did not follow first order kinetics but could be fitted using the Korsmeyer−Peppas approximation with values for the release exponent (n) similar to those reported for drug-loaded liposomes that was diffusion limited (n = 0.2−0.3).[39,40] Release from 10 wt % loaded worms with various surface compositions (U/A/CA) was comparable and proceeded to full release over 3 days (as compared to ca. 10 h with spherical micelles). In part, this observed difference was attributed to the higher loading of DEX in worms and the concomitant (relative) reduction in drug efflux as $[DEX]_{worms} > [DEX]_{solubility}$. Reducing the loading of DEX in worms highlighted this property, where 8 and 6 wt % worms showed a reduction in the release exponent and an increase in the rate constant, highlighting faster release when $[DEX]_{worms} \approx [DEX]_{solubility}$. Overall, high aspect ratio nanoparticles, by definition nonspherical, demonstrated their capacity to reduce the rate of drug release; for worm-like micelles, with higher loading content of drug, this was even significantly enhanced.

Following on from *in vitro* studies, we explored the impact of particle shape and surface chemistry on mobility in the vitreous using *ex vivo* porcine eyes, an excellent model system due to similarity to the human eye.[41] After addition to a prepared eye, fluorescent nanoparticles with Bodipy-FL dye were tracked as they underwent diffusion within the gel-like vitreous fluid. Particle mobility was quantified using the ratio of diffusion coefficients (D_w/D_v) measured in water (D_w, using the

https://dx.doi.org/10.1021/acs.biomac.0c00726
Biomacromolecules 2021, 22, 126−133

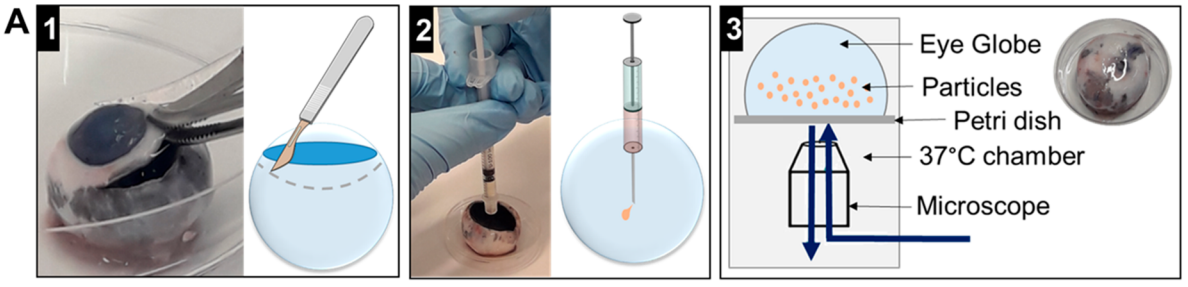

C

FAST	Dw/Dv ratio						SLOW
4.98	5.23	12.8	17.1	17.1	18.8	27.0	31.3
CA-worm	Worm	CA-tube	CA-sphere	Tube	A-tube	A-sphere	Sphere

Figure 3. Diffusion of diverse nanoparticle morphologies *in vitreous*. (A) Scheme for the preparation and sample measurement in an *ex vivo* eye model. (B) Example of nanoparticle mobility trajectories in the *ex vivo* eye as measured using confocal microscopy and processed using Imaris software. (C) Chart of D_w/D_v ratios for diverse particle morphologies.

Stokes–Einstein equation) compared to that measured in vitreous fluid (D_v, extracted from mean-squared displacement, MSD) as described in the methods.[33] MSDs of particles were calculated from tracked trajectories to provide mobility ratio (D_w/D_v) values (Figures 3 and S13 and Videos 7–14). Both surface composition and shape had a clear effect on particle mobility in vitreous fluid. In terms of surface composition, CA-modified particles showed enhanced diffusion in the vitreous as compared to U or A-modified variants, which can be explained by negative interactions with anionic polysaccharides such as hyaluronic acid. In terms of shape, tubular polymersomes were clearly more mobile than spheres with ratio values at between 55 and 75% that of spheres. Due to the gel-like environment of the vitreous, 100 nm-wide tubular shapes (as opposed to bulky spheres) likely possessed enhanced diffusion due to their ability to transverse the vitreal gel more effectively than spheres. In line with this logic, worm-like micelles (having significantly greater aspect ratio as compared to tubes) yielded diffusion ratio values over threefold lower than those of tubes, thus diffusing faster. These observations give additional insight into the enhanced cellular uptake of tubes and worms (particularly those with CA-modified surfaces) that can be related to their enhanced mobility *in vitreous*, increasing the degree of cell interactions in agreement with the literature.[10] As a proof-of-principal and to highlight the ability of nonspherical morphologies to enhance penetration of complex biological barriers, fluorescently labeled CA-tubes were shown to penetrate the inner limiting membrane (ILM) of the retina (Figure S14). Even though absolute conclusions could not be drawn from those images, the ability of elongated nanoparticles to transpose such an interface highlights their value for further exploration for a potential retinal application.

CONCLUSION

In conclusion, we demonstrated that nanoparticle morphology is an important factor in the design of drug delivery systems due to its impact on behavior such as cell uptake, drug release kinetics, and diffusion in complex biological media. High aspect ratio nanostructures (such as tubular polymersomes and worm-like micelles) have great potential for further development toward therapeutic applications (such as ocular therapy). In combination with computational modeling, the use of such morphologically diverse nanoparticles would deepen our understanding of the role of parameters such as size, shape, and composition upon interactions with biological interfaces and cells.

ASSOCIATED CONTENT

Supporting Information

The Supporting Information is available free of charge at https://pubs.acs.org/doi/10.1021/acs.biomac.0c00726.

Video in 3D of U-sphere nanoparticles uptaken by ARPE-19 cells (MP4)

Video in 3D of A-sphere nanoparticles uptaken by ARPE-19 cells (MP4)

Video in 3D of CA-sphere nanoparticles uptaken by ARPE-19 cells (MP4)

Video in 3D of U-tube nanoparticles uptaken by ARPE-19 cells (MP4)

https://dx.doi.org/10.1021/acs.biomac.0c00726
Biomacromolecules 2021, 22, 126–133

Video in 3D of A-tube nanoparticles uptaken by ARPE-19 cells (MP4)
Video in 3D of CA-tube nanoparticles uptaken by ARPE-19 cells (MP4)
Video of U-sphere nanoparticles mobility in ex vivo eye (MP4)
Video of A-sphere nanoparticles mobility in ex vivo eye (MP4)
Video of CA-sphere nanoparticles mobility in ex vivo eye (MP4)
Video of U-tube nanoparticles mobility in ex vivo eye (MP4)
Video of A-tube nanoparticles mobility in ex vivo eye (MP4)
Video of CA-tube nanoparticles mobility in ex vivo eye (MP4)
Video of U-worm nanoparticles mobility in ex vivo eye (MP4)
Video of CA-worm nanoparticles mobility in ex vivo eye (MP4)
Polymer synthesis and characterizations by NMR and GPC, particles characterizations by DLS and CryoTEM, cell uptake of particles by FACS, confocal imaging, 3D experiments, drug loading and release experiments, and particle mobility and permeation in *ex vivo* eye (PDF)

AUTHOR INFORMATION

Corresponding Authors

Jan C. M. van Hest − *Bio-Organic Chemistry, Institute for Complex Molecular Systems, Eindhoven University of Technology, 5600 MB Eindhoven, The Netherlands;* orcid.org/0000-0001-7973-2404; Email: j.c.m.v.hest@tue.nl

David S. Williams − *Department of Chemistry, College of Science, Swansea University, Swansea SA2 8PP, United Kingdom;* orcid.org/0000-0002-8209-6899; Email: d.s.williams@swansea.ac.uk

Arto Urtti − *Drug Research Program, Faculty of Pharmacy, University of Helsinki, 00790 Helsinki, Finland;* orcid.org/0000-0001-6064-3102; Email: arto.urtti@helsinki.fi

Authors

Roxane Ridolfo − *Bio-Organic Chemistry, Institute for Complex Molecular Systems, Eindhoven University of Technology, 5600 MB Eindhoven, The Netherlands*

Shirin Tavakoli − *Drug Research Program, Faculty of Pharmacy, University of Helsinki, 00790 Helsinki, Finland*

Vijayabhaskarreddy Junnuthula − *Drug Research Program, Faculty of Pharmacy, University of Helsinki, 00790 Helsinki, Finland*

Complete contact information is available at: https://pubs.acs.org/10.1021/acs.biomac.0c00726

Notes

The authors declare no competing financial interest.

ACKNOWLEDGMENTS

Thanks to Imke Pijpers-Welzen and Alexander Mason (TU/e, Eindhoven) for their assistance with CryoTEM imaging. Thanks to Timo J. Oksanen (Univ. Helsinki) for UPLC measurements. Thanks to Conor Horgan and Jelle Penders (Imperial College London) for their cell staining protocol. We thank the European Union's Horizon 2020 research and innovation program Marie Sklodowska-Curie Innovative Training Networks (ITN) Nanomed (Grant 676137) for support of R.R., V.J., and S.T. We thank the Ser Cymru II programme for support of D.S.W.; this project received funding from the European Union's Horizon 2020 research and innovation programme under the Marie Skłodowska-Curie Grant 663830.

REFERENCES

(1) Williams, D. S.; Pijpers, I. A. B.; Ridolfo, R.; van Hest, J. C. M. Controlling the Morphology of Copolymeric Vectors for next Generation Nanomedicine. *J. Controlled Release* **2017**, *259*, 29−39.
(2) Massignani, M.; LoPresti, C.; Blanazs, A.; Madsen, J.; Armes, S. P.; Lewis, A. L.; Battaglia, G. Controlling Cellular Uptake by Surface Chemistry, Size, and Surface Topology at the Nanoscale. *Small* **2009**, *5* (21), 2424−2432.
(3) Euliss, L. E.; DuPont, J. A.; Gratton, S.; DeSimone, J. Imparting Size, Shape, and Composition Control of Materials for Nanomedicine. *Chem. Soc. Rev.* **2006**, *35* (11), 1095−1104.
(4) Allert, M. J.; Hellinga, H. W. Describing Complex Structure-Function Relationships in Biomolecules at Equilibrium. *J. Mol. Biol.* **2020**, *432* (7), 1926−1951.
(5) Bush, L. M.; Gibbs, C.; Deans, T. L. Synthetic Biology Synthetic Biology: Paving the Way with Novel Drug Delivery. *Synth. Biol.* **2019**, *41* (3), 24−27.
(6) Mann, S. Life as a Nanoscale Phenomenon. *Angew. Chem., Int. Ed.* **2008**, *47* (29), 5306−5320.
(7) Shafaie, S.; Hutter, V.; Cook, M. T.; Brown, M. B.; Chau, D. Y. S. *In Vitro* Cell Models for Ophthalmic Drug Development Applications. *BioRes. Open Access* **2016**, *5* (1), 94−108.
(8) Fletcher, E. L.; Jobling, A. I.; Vessey, K. A.; Luu, C.; Guymer, R. H.; Baird, P. N. Animal Models of Retinal Disease. *Prog. Mol. Biol. Transl. Sci.* **2011**, *100*, 211−286.
(9) Zhang, K.; Zhang, L.; Weinreb, R. N. Ophthalmic Drug Discovery: Novel Targets and Mechanisms for Retinal Diseases and Glaucoma. *Nat. Rev. Drug Discovery* **2012**, *11* (7), 541−559.
(10) del Amo, E. M.; Rimpelä, A. K.; Heikkinen, E.; Kari, O. K.; Ramsay, E.; Lajunen, T.; Schmitt, M.; Pelkonen, L.; Bhattacharya, M.; Richardson, D.; Subrizi, A.; Turunen, T.; Reinisalo, M.; Itkonen, J.; Toropainen, E.; Casteleijn, M.; Kidron, H.; Antopolsky, M.; Vellonen, K. S.; Ruponen, M.; Urtti, A. Pharmacokinetic Aspects of Retinal Drug Delivery. *Prog. Retinal Eye Res.* **2017**, *57*, 134−185.
(11) Thrimawithana, T. R.; Young, S.; Bunt, C. R.; Green, C.; Alany, R. G. Drug Delivery to the Posterior Segment of the Eye. *Drug Discovery Today* **2011**, *16* (5−6), 270−277.
(12) Grzybowski, A.; Told, R.; Sacu, S.; Bandello, F.; Moisseiev, E.; Loewenstein, A.; Schmidt-Erfurth, U. 2018 Update on Intravitreal Injections: Euretina Expert Consensus Recommendations. *Ophthalmologica* **2018**, *239* (4), 181−193.
(13) Mitchell, P.; Liew, G.; Gopinath, B.; Wong, T. Y. Age-Related Macular Degeneration. *Lancet* **2018**, *392* (11), 1147−1159.
(14) Thakur, S. S.; Barnett, N. L.; Donaldson, M. J.; Parekh, H. S. Intravitreal Drug Delivery in Retinal Disease: Are We out of Our Depth? *Expert Opin. Drug Delivery* **2014**, *11* (10), 1575−1590.
(15) Wong, W. L.; Su, X.; Li, X.; Cheung, C. M. G.; Klein, R.; Cheng, C. Y.; Wong, T. Y. Global Prevalence of Age-Related Macular Degeneration and Disease Burden Projection for 2020 and 2040: A Systematic Review and Meta-Analysis. *Lancet Glob. Heal.* **2014**, *2*, 106−116.
(16) Birch, D. G.; Liang, F. Q. Age-Related Macular Degeneration: A Target for Nanotechnology Derived Medicines. *Int. J. Nanomed.* **2007**, *2* (1), 65−77.
(17) Le Goff, M.; Bishop, P. Adult Vitreous Structure and Postnatal Changes. *Eye* **2008**, *22*, 1214−1222.
(18) Geng, Y.; Dalhaimer, P.; Cai, S.; Tsai, R.; Tewari, M.; Minko, T.; Discher, D. E. Shape Effects of Filaments versus Spherical Particles in Flow and Drug Delivery. *Nat. Nanotechnol.* **2007**, *2* (4), 249−255.

(19) Gentile, F.; Chiappini, C.; Fine, D.; Bhavane, R. C.; Peluccio, M. S.; Cheng, M. M. C.; Liu, X.; Ferrari, M.; Decuzzi, P. The Effect of Shape on the Margination Dynamics of Non-Neutrally Buoyant Particles in Two-Dimensional Shear Flows. *J. Biomech.* **2008**, *41*, 2312−2318.
(20) Lee, S. Y.; Ferrari, M.; Decuzzi, P. Design of Bio-Mimetic Particles with Enhanced Vascular Interaction. *J. Biomech.* **2009**, *42* (12), 1885−1890.
(21) Decuzzi, P.; Pasqualini, R.; Arap, W.; Ferrari, M. Intravascular Delivery of Particulate Systems: Does Geometry Really Matter? *Pharm. Res.* **2009**, *26* (1), 235−243.
(22) Champion, J. A.; Mitragotri, S. Role of Target Geometry in Phagocytosis. *Proc. Natl. Acad. Sci. U. S. A.* **2006**, *103* (13), 4930−4934.
(23) Pitkänen, L.; Ruponen, M.; Nieminen, J.; Urtti, A. Vitreous Is a Barrier in Nonviral Gene Transfer by Cationic Lipids and Polymers. *Pharm. Res.* **2003**, *20* (4), 576−583.
(24) Pitkänen, L.; Pelkonen, J.; Ruponen, M.; Rönkkö, S.; Urtti, A. Neural Retina Limits the Nonviral Gene Transfer to Retinal Pigment Epithelium in an in Vitro Bovine Eye Model. *AAPS J.* **2004**, *6* (3), 1−9.
(25) Koo, H.; Moon, H.; Han, H.; Na, J. H.; Huh, M. S.; Park, J. H.; Woo, S. J.; Park, K. H.; Chan Kwon, I.; Kim, K.; Kim, H. The Movement of Self-Assembled Amphiphilic Polymeric Nanoparticles in the Vitreous and Retina after Intravitreal Injection. *Biomaterials* **2012**, *33*, 3485−3493.
(26) Chang-Lin, J. E.; Attar, M.; Acheampong, A. A.; Robinson, M. R.; Whitcup, S. M.; Kuppermann, B. D.; Welty, D. Pharmacokinetics and Pharmacodynamics of a Sustained-Release Dexamethasone Intravitreal Implant. *Invest. Ophthalmol. Visual Sci.* **2011**, *52* (1), 80−86.
(27) Bansal, R.; Bansal, P.; Kulkarni, P.; Gupta, V.; Sharma, A.; Gupta, A. Wandering Ozurdex® Implant. *J. Ophthalmic Inflammation Infect.* **2012**, *2*, 1−5.
(28) Pardo-López, D.; Francés-Muñoz, E.; Gallego-Pinazo, R.; Díaz-Llopis, M. Anterior Chamber Migration of Dexametasone Intravitreal Implant (Ozurdex®). *Graefe's Arch. Clin. Exp. Ophthalmol.* **2012**, *250*, 1703−1704.
(29) Ridolfo, R.; Ede, B. C.; Diamanti, P.; White, P. B.; Perriman, A. W.; van Hest, J. C. M.; Blair, A.; Williams, D. S. Biodegradable, Drug-Loaded Nanovectors via Direct Hydration as a New Platform for Cancer Therapeutics. *Small* **2018**, *14* (32), 1−10.
(30) Ridolfo, R.; Williams, D. S.; van Hest, J. C. M. Influence of Surface Charge on the Formulation of Elongated PEG-b-PDLLA Nanoparticles. *Polym. Chem.* **2020**, *11*, 2775−2780.
(31) Ridolfo, R.; Arends, J. J.; van Hest, J. C. M.; Williams, D. S. Worm-like Nanovector with Enhanced Drug Loading Using Blends of Biodegradable Block Copolymers. *Biomacromolecules* **2020**, *21*, 2199.
(32) Abdelmohsen, L. K. E. A.; Williams, D. S.; Pille, J.; Ozel, S. G.; Rikken, R. S. M.; Wilson, D. A.; Van Hest, J. C. M. Formation of Well-Defined, Functional Nanotubes via Osmotically Induced Shape Transformation of Biodegradable Polymersomes. *J. Am. Chem. Soc.* **2016**, *138* (30), 9353−9356.
(33) Subia, B.; Reinisalo, M.; Dey, N.; Tavakoli, S.; Subrizi, A.; Ganguli, M.; Ruponen, M. Nucleic Acid Delivery to Differentiated Retinal Pigment Epithelial Cells Using Cell-Penetrating Peptide as a Carrier. *Eur. J. Pharm. Biopharm.* **2019**, *140*, 91−99.
(34) Rimpelä, A. K.; Reunanen, S.; Hagström, M.; Kidron, H.; Urtti, A. Binding of Small Molecule Drugs to Porcine Vitreous Humor. *Mol. Pharmaceutics* **2018**, *15* (6), 2174−2179.
(35) Wang, J.; Yang, Y.; Yu, M.; Hu, G.; Gan, Y.; Gao, H.; Shi, X. Diffusion of Rod-like Nanoparticles in Non-Adhesive and Adhesive Porous Polymeric Gels. *J. Mech. Phys. Solids* **2018**, *112*, 431−457.
(36) Peynshaert, K.; Devoldere, J.; De Smedt, S. C.; Remaut, K. In Vitro and Ex Vivo Models to Study Drug Delivery Barriers in the Posterior Segment of the Eye. *Adv. Drug Delivery Rev.* **2018**, *126*, 44−57.
(37) Wang, J.; Mao, W.; Lock, L. L.; Tang, J.; Sui, M.; Sun, W.; Cui, H.; Xu, D.; Shen, Y. The Role of Micelle Size in Tumor Accumulation, Penetration, and Treatment. *ACS Nano* **2015**, *9* (7), 7195−7206.
(38) Pekker, M.; Shneider, M. Interaction between Electrolyte Ions and the Surface of a Cell Lipid Membrane. *J. Phys. Chem. Biophys.* **2015**, *5* (2), 177−184.
(39) Haghiralsadat, F.; Amoabediny, G.; Helder, M. N.; Naderinezhad, S.; Sheikhha, M. H.; Forouzanfar, T.; Zandieh-Doulabi, B. A Comprehensive Mathematical Model of Drug Release Kinetics from Nano-Liposomes, Derived from Optimization Studies of Cationic PEGylated Liposomal Doxorubicin Formulations for Drug-Gene Delivery. *Artif. Cells, Nanomed., Biotechnol.* **2018**, *46* (1), 169−177.
(40) Jain, A.; Jain, S. K. In Vitro Release Kinetics Model Fitting of Liposomes: An Insight. *Chem. Phys. Lipids* **2016**, *201*, 28−40.
(41) Pennesi, M. E.; Neuringer, M.; Courtney, R. J. Animal Models of Age Related Macular Degeneration. *Mol. Aspects Med.* **2012**, *33* (4), 487−509.

https://dx.doi.org/10.1021/acs.biomac.0c00726
Biomacromolecules 2021, 22, 126−133